Monthly Notices
of the
ROYAL ASTRONOMICAL SOCIETY

MNRAS **510,** 1649–1656 (2022)
Advance Access publication 2021 December 3

https://doi.org/10.1093/mnras/stab3481

Rate coefficients of the aluminium monoxide formation by radiative association

Tianrui Bai,[1,2] Zhi Qin [2,3]★ and Linhua Liu [1,2,4]★

[1]*School of Energy and Power Engineering, Shandong University, Jinan, Shandong 250061, China*
[2]*Optics and Thermal Radiation Research Center, Institute of Frontier and Interdisciplinary Science, Shandong University, Qingdao, Shandong 266237, China*
[3]*School of Information Science and Engineering, Shandong University, Qingdao, Shandong 266237, China*
[4]*School of Energy Science and Engineering, Harbin Institute of Technology, Harbin, Heilongjiang 150001, China*

Accepted 2021 November 22. Received 2021 November 14; in original form 2021 September 19

ABSTRACT

Radiative association may be a key pathway for the formation of aluminium monoxide (AlO) in diffuse interstellar clouds, especially for the oxygen-rich asymptotic giant branch (AGB) stars. In this work, we investigated the radiative association of AlO by the collision of the aluminium and oxygen atoms in their electronic ground states, which is thought to be the most probable radiative association process. First, the potential energy curves for 12 electronic states and the dipole moments between these states were calculated by the state-of-the-art *ab initio* methodology. Then, the cross-sections and rate coefficients for the radiative association of AlO were computed for the temperatures in the range of 10–10 000 K. The total rate coefficients are of the order of 2.73×10^{-19}–1.14×10^{-16} cm^3 s^{-1}, and the $A^2\Pi \rightarrow X^2\Sigma^+$, $1^2\Delta \rightarrow A^2\Pi$, $1^2\Pi \rightarrow X^2\Sigma^+$, and $2^2\Sigma^- \rightarrow A^2\Pi$ transitions play a key role. The calculated results can be used to investigate the chemical evolution of dust formation in the photospheres of the oxygen-rich AGB stars.

Key words: astrochemistry – molecular data – molecular processes.

1 INTRODUCTION

Aluminium monoxide (AlO) has long been a topic of interest for its astrophysical importance, since most studies assume the simplest oxide is the primitive gas precursor of alumina seeds. Thus, it can be used to trace the aluminium oxide (Al_2O_3) dust formation site in the high-temperature region near many oxygen-rich asymptotic giant branch (AGB) stars and open pathways to the formation of aluminium oxide clusters (Onaka, De Jong & Willems 1989; Speck et al. 2000; Van Heijnsbergen et al. 2003). So far, AlO molecules have been detected around oxygen-rich supergiants (Takigawa et al. 2017), VY Canis Majoris (Tenenbaum & Ziurys 2009), Mira variables (Merrill, Deutsch & Keenan 1962; Keenan, Deutsch & Garrison 1969), and R Aquarii (De Beck et al. 2017) at (sub)millimetre wavelengths.

Aluminium oxide is considered to play a significant role in dust formation (Banerjee et al. 2007), but it still has remained a significant conundrum as to how the processes control the formation of aluminium oxide dust. Therefore, as the abundant gas precursor, the formation process of AlO is required to investigate the evolution of aluminium oxide dust in the high-temperature circumstellar environments. One possible formation mechanism is the radiative association reaction $Al + O \rightarrow AlO + h\nu$, which has been considered in many chemical networks of dust formation in the oxygen-rich AGB star (Cherchneff & Lilly 2008; Sarangi & Cherchneff 2013; Gobrecht et al. 2016). In addition, atomic oxygen is very abundant in the O-rich zones, and its inclusion in clusters can proceed through slow reactions such as termolecular (cluster + O + M → [cluster + O] + M) and radiative association (cluster + O → [cluster + O] + *hν*) processes (Sarangi & Cherchneff 2013).

To accurately model the chemical networks of the alumina dust formation, the rate coefficients for radiative association processes of Al-containing molecules, such as AlO, AlN, AlF, and AlCl, have been calculated by a semiclassical (SC) method (Ceccatto 2012; Andreazza & de Almeida 2014; Andreazza, de Almeida & Vichietti 2018). These rates can be viewed as the direct contribution but the indirect contribution was not considered, which arises primarily from quantum mechanical (QM) tunnelling through the barrier in the effective potential but also from 'overbarrier' resonances (Nyman, Gustafsson & Antipov 2015). Besides, in the calculation of Ceccatto (2012), the extrapolated potential energy curves (PECs) from experimental data were used. However, only low-lying electronic states and low-energy levels have been measured in experiments, thus leading to the inaccurate and incomplete results of rates for AlO radiative association. In this work, we employ the state-of-the-art *ab initio* methodology to determine the PECs and the QM theory to calculate the rate coefficients for the radiative association of AlO. Both the direct and indirect contributions have been obtained by the QM theory.

For the radiative association process of AlO, we consider the collision of the aluminium and oxygen atoms in their electronic ground states, which is thought to be the most probable radiative association process (Ceccatto 2012). Therefore, 12 electronic states are produced. The strong spin-allowed transitions between these states are chosen to calculate the cross-sections and rate coefficients.

★ E-mail: z.qin@sdu.edu.cn (ZQ); liulinhua@sdu.edu.cn (LL)

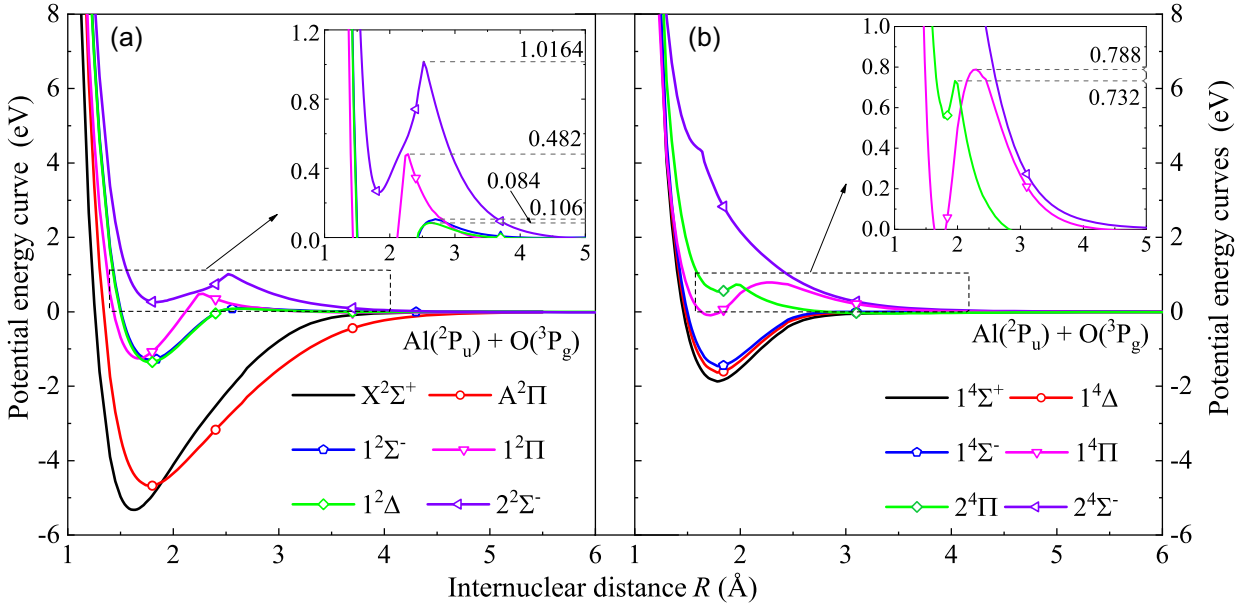

Figure 1. The PECs of the (a) $X^2\Sigma^+$, $A^2\Pi$, $1^2\Delta$, $1^2\Sigma^-$, $1^2\Pi$, and $2^2\Sigma^-$ states and (b) $1^4\Sigma^+$, $1^4\Delta$, $1^4\Pi$, $1^4\Sigma^-$, $2^4\Pi$, and $2^4\Sigma^-$ states for AlO.

2 METHODS

2.1 Potential energy and transition moment curves

The complete active space self-consistent field (CASSCF) method (Knowles & Werner 1985) in conjunction with the subsequent internally contracted MRCI approach (Knowles & Werner 1988; Werner & Knowles 1988) with the Davidson correction (icMRCI + Q) is used for the main calculations of the PECs with the aug-cc-pCV5Z-DK basis set, including the core–valance correction (Woon & Dunning 1995) and scalar relativistic correction (de Jong, Harrison & Dixon 2001). The transition dipole moments (TDMs) and permanent dipole moments (PDMs) are also computed by the icMRCI + Q method with the aug-cc-pCV5Z-DK basis set. These calculations are performed in the MOLPRO 2015 program package (Werner et al. 2015).

In the calculations, 12 inner electrons are put into six closed-shell molecular orbitals (MOs) in the symmetry representations of C_2: four a_1 orbitals, one b_1 orbital, one b_2 orbital, and no a_2 orbitals. The remaining nine electrons are put into eight outermost MOs, which constitute the active space: four a_1 orbitals, two b_1 orbital, two b_2 orbital, and no a_2 orbitals. The orbital set is called (8, 3, 3, 0). Using the obtained PECs, we can determine the dissociation energy D_e, the electronic excitation energy with respect to the ground state T_e, the harmonic frequency ω_e, the vibration coupling constant α_e, the rotational constant B_e, and the first-order anharmonic constants $\omega_e\chi_e$.

To calculate the cross-sections, the PECs, TDMs, and PDMs are required to be extrapolated over short and long ranges of internuclear distances R. At large distances ($R > 13$ Å), the PECs are extrapolated by the following function:

$$V(R) = -\frac{C_5}{R^5} - \frac{C_6}{R^6} + V(R \to \infty), \tag{1}$$

where C_5 is the quadrupole–quadrupole electrostatic interaction and can be estimated by the method proposed by Chang (1967). For example, we used $C_5 = -39.67$ for the $X^2\Sigma^+$ and $1^4\Sigma^+$ states, 26.45 for the $1^2\Pi$ and $2^4\Pi$ states, and -6.61 for the $1^2\Delta$ and $1^4\Delta$ states. C_6 is the dipole–dipole dispersion (van der Waals) coefficient and can be calculated by the London formula (London 1937)

$$C_6 = \frac{3}{2}\frac{\tau_{Al}\tau_O}{\tau_{Al}+\tau_O}\alpha_{Al}\alpha_O, \tag{2}$$

where τ is the ionization energy of the atom, which can be obtained from the NIST Atomic Spectra Data base (Kramida et al. 2021). α is the static dipole polarizability. Based on the coupled-cluster calculations, the polarizabilities of 5.24 and 58.44 au are calculated for the ground states of the oxygen and aluminium atoms, respectively (Das & Thakkar 1999; Fuentealba 2004). Therefore, $C_6 = 70.20$ is obtained. For the short ranges, the PECs can be extrapolated to zero by the function $V(R) = A\exp(-BR) + C$. The same extrapolation is used for the TDMs and PDMs.

2.2 Cross-sections and rate coefficients

The total rate coefficient α_{tot} for the formation of a bound molecule can be calculated by averaging cross-sections over a Maxwellian velocity distribution and given by

$$\begin{aligned}\alpha_{tot}(T) &= \sum_{\Lambda\to\Lambda'}\alpha_{\Lambda\to\Lambda'}(T)\\ &= \sum_{\Lambda\to\Lambda'}\sqrt{\frac{8}{\pi\mu(k_BT)^3}}\int_0^\infty E\sigma_{\Lambda\to\Lambda'}(E)e^{(-E/k_BT)}dE,\end{aligned} \tag{3}$$

where $\alpha_{\Lambda\to\Lambda'}(T)$ are the rate coefficients for the specific electronic transition process, $\Lambda \to \Lambda'$. μ is the reduced mass. $\sigma_{\Lambda\to\Lambda'}(E)$ is the cross-section, as a function of the collision energy E. Based on the light-matter interactions and thermodynamic relations for the Einstein coefficient describing the spontaneous emission of a photon, the cross-sections can be computed by the QM method (Golubev et al. 2013; Nyman et al. 2015)

$$\begin{aligned}&\sigma_{\Lambda\to\Lambda'} =\\ &\sum_{J;v',J'}\frac{1}{4\pi\varepsilon_0}\frac{64}{3}\frac{\pi^5}{k^2}\left(\frac{v}{c}\right)^3 f_\Lambda S_{\Lambda,J\to\Lambda',J'}|\langle\chi_{E,J}(R)|D(R)\psi_{v',J'}(R)\rangle|^2,\end{aligned} \tag{4}$$

Table 1. Spectroscopic parameters of electronic states of AlO obtained by the icMRCI + Q method.

States		T_e	R_e	ω_e (cm^{-1})	$\omega_e\chi_e$ (cm^{-1})	B_e (cm^{-1})	$10^3\alpha_e$ (cm^{-1})
$X^2\Sigma^+$	This work	0	1.625	982.09	7.72	0.6361	5.45
	Expt[a]	0	1.6179	979.23	6.97	0.6413	5.8
	Expt[b]	0	1.6178	979.49	7.012	0.6414	5.78
	Expt[c]	0		979.52	7.036	0.6417	5.934
	Calc[d]	0	1.6092	989.2	11.97		
	Calc[e]	0	1.6156	1028.9	5.45	0.644	
	Calc[f]	0	1.635	1169.2	4.2	0.624	3.2
	Calc[g]	0	1.623	977	6.8		
	Calc[h]	0	1.628	970	6.3		
	Calc[i]	0	1.6207	979.23	7.0509	0.6403	6.402
$A^2\Pi$	This work	5234	1.770	739.69	5.95	0.5281	4.12
	Expt[a]	5341.7	1.7708	728.5	4.15	0.5333	
	Expt[b]	5407.73	1.7678	729.7	4.476	0.5372	5.002
	Calc[d]	2819	1.7648	747.4	4.96		
	Calc[j]	3318.0	1.7780	762			
	Calc[g]	5050	1.777	7204.18			
	Calc[i]	5190.4	1.7620	723.44	2.1823	0.5450	12.609
$1^2\Delta$	This work	32 028	1.776	748.58	8.23	0.5257	4.23
	Calc[k]	34 750	1.747	816			
	Calc[g]	31 852	1.786	719			
$1^2\Sigma^-$	This work	32 507	1.783	737.22	7.08	0.5252	4.49
	Calc[k]	34 950	1.747	851			
	Calc[g]	32 351	1.791	716			
$1^2\Pi$	This work	32 853	1.674	867.81	8.3090	0.6007	5.84
	Expt[l]	33 047	1.671	856		0.6007	
	Calc[g]	32 875	1.679	846			
$1^4\Sigma^+$	This work	27 884	1.787	770.30	7.71	0.5289	4.75
	Calc[k]	33 100	1.723	581			
	Calc[g]	27 222	1.776	723			
	Calc[i]	26 781.8	1.7591	770.11	5.3183	0.5426	4.910
$1^4\Delta$	This work	29 807	1.787	768.49	9.0411	0.524 45	6.79
	Calc[k]	31 700	1.750	834			
	Calc[g]	29 350	1.785	699			
$1^4\Pi$	This work	42 228	1.710	752.94	11.12	0.5717	5.83
	Calc[k]	43 800	1.705	805			
	Calc[g]	41 190	1.72	768			
	Calc[i]	42 060.3	1.6962	755.64	5.7260	0.5835	5.752
$1^4\Sigma^-$	This work	31 168	1.794	737.91	7.34	0.5226	9.37
	Calc[k]	33 100	1.756	820			
	Calc[g]	30 678	1.788	690			

Note.[a] Huber & Herzberg (1979), [b] Launila & Jonsson (1994), [c] Saksena et al. (2008), [d] Yoshimine, McLean & Liu (1973), [e] Lengsfield & Liu (1982), [f] Kovba & Topol (1986), [g] Zenouda et al. (1999), [h] Honjou (2010), [i] Liu et al. (2013), [j] Partridge et al. (1983), [k] Schamps (1973), and [l] Towle et al. (1994).

Table 2. Transitions studied in this work.

Initial state	to	Final state	Initial state	to	Final state
$1^2\Pi$	→	$A^2\Pi$	$2^4\Pi$	→	$1^4\Delta$
$A^2\Pi$	→	$X^2\Sigma^+$	$2^4\Pi$	→	$1^4\Sigma^+$
$X^2\Sigma^+$	→	$A^2\Pi$	$1^4\Delta$	→	$1^4\Delta$
$1^2\Pi$	→	$X^2\Sigma^+$	$1^4\Sigma^+$	→	$1^4\Sigma^+$
$1^2\Delta$	→	$A^2\Pi$	$1^4\Sigma^-$	→	$1^4\Sigma^-$
$1^2\Sigma^-$	→	$A^2\Pi$	$2^4\Pi$	→	$1^4\Sigma^-$
$2^2\Sigma^-$	→	$A^2\Pi$	$1^4\Pi$	→	$1^4\Delta$
$A^2\Pi$	→	$A^2\Pi$	$1^4\Pi$	→	$1^4\Sigma^+$
$X^2\Sigma^+$	→	$X^2\Sigma^+$	$1^4\Pi$	→	$1^4\Sigma^-$
$1^2\Pi$	→	$1^2\Sigma^-$			

where ε_0 is the vacuum permittivity, $k^2 = 2\mu E/\hbar^2$, and $S_{\Lambda,J\to\Lambda',J'}$ is the Hönl–London factor (Hansson & Watson 2005; Watson 2008). f_Λ is the probability of approach in the initial electronic state. $D(R)$ are the *ab initio* TDMs or PDMs, $\chi_{E,J}(R)$ are the normalized wavefunctions of the initial continuum state, and $\psi_{v',J'}(R)$ are the bound wavefunctions of the final state. The continuum and bound wavefunctions can be obtained by the renormalized Numerov method (Johnson 1977, 1978).

To verify the cross-sections calculated by QM method, the SC method is employed and the cross-sections can be calculated by

$$\sigma_{\Lambda\to\Lambda'}(E) = 4\pi\sqrt{\frac{\mu}{2E}}f_\Lambda\int_0^\infty b\,\mathrm{d}b\int_{R_c}^\infty \frac{A^{Eb}_{\Lambda\to\Lambda'}(R)}{\sqrt{1-\frac{V_\Lambda(R)}{E}-\frac{b^2}{R^2}}}\mathrm{d}R, \quad (5)$$

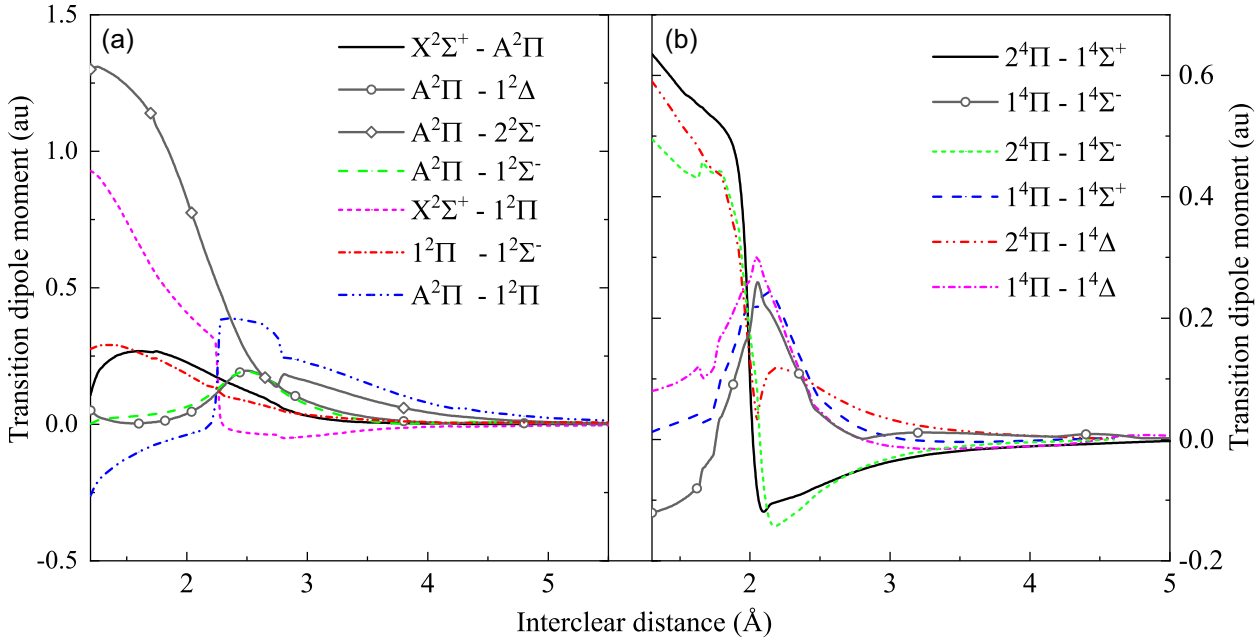

Figure 2. The TDMs for 13 dipole allowed transition systems between (a) doublet and (b) quartet states.

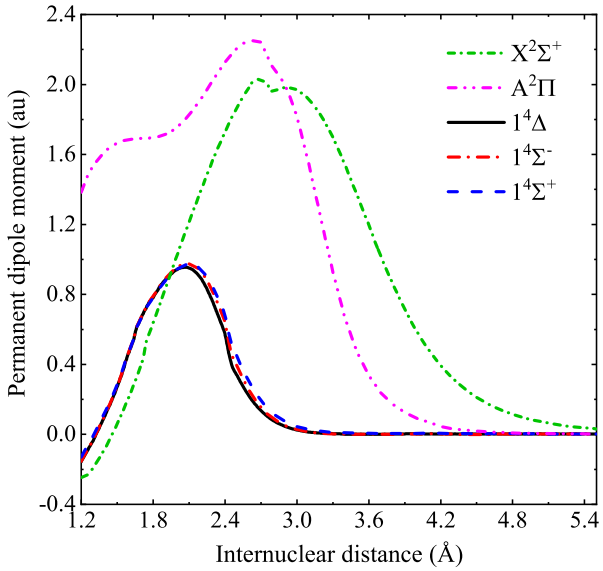

Figure 3. The PDMs of the $X^2\Sigma^+$, $A^2\Pi$, $1^4\Delta$, $1^4\Sigma^-$, and $1^4\Sigma^+$ states.

where b is the impact parameter, R_c is the outer turning point, and $A_{\Lambda\to\Lambda'}$ is the transition rate for the spontaneous emission. More details about these parameters can refer to Nyman et al. (2015).

3 RESULTS AND DISCUSSION

3.1 Potential energy curves and transition dipole moments

The PECs of 12 electronic states for AlO are calculated at the icMRCI + Q/aug-cc-pCV5Z-DK level of theory and plotted in Fig. 1. The PECs of the $1^2\Delta$ and $1^2\Sigma^-$ states are extremely similar. This is because the electron configurations of both states have nearly the same weigh. The fitted spectroscopic parameters are summarized in Table 1, along with the experimental and theoretical results. For the $X^2\Sigma^+$, $A^2\Pi$, and $1^2\Pi$ states, our calculated spectroscopic parameters are in quite good agreement with those determined experimentally (Huber & Herzberg 1979; Launila & Jonsson 1994; Saksena et al. 2008). The T_e, R_e, and ω_e values differ by a maximum of 194 cm^{-1}, 0.0072 Å, and 11.81 cm^{-1}, respectively. The $1^2\Delta$ and $1^2\Sigma^-$ states have nearly the same PECs, thus resulting in similar spectroscopic parameters. The spectroscopic parameters calculated in this work also agree well with the relatively recent ones computed by Zenouda et al. (1999). For the quartet states, they have not been identified in the experiments so far, but our computed T_e and ω_e values are within the range of other theoretical results (Schamps 1973; Zenouda et al. 1999; Liu et al. 2013).

There are numerous spin-allowed electric dipole transitions within the calculated electronic states, but the radiative association cross-sections depend on the square of the dipole moments and the third power of the electronic transition energies. Accordingly, the allowed transitions with large transition energies and dipole moments are chosen to be considered in this work, as listed in Table 2. Utilizing the icMRCI method with the aug-cc-pCV5Z-DK basis set, the TDMs and PDMs for the considered transitions between doublet and quartet states are computed, as shown in Figs 2 and 3. The TDMs of the $1^2\Delta \to A^2\Pi$ and $1^2\Sigma^- \to A^2\Pi$ systems are very similar, which is consistent with the similar electron configurations ($5\sigma^2 6\sigma^2 2\pi^3 7\sigma^1 3\pi^1$) of the $1^2\Delta$ and $1^2\Sigma^-$ states around their corresponding equilibrium internuclear distances.

3.2 Cross-sections

To verify the results obtained by the QM method, the cross-sections for the $A^2\Pi \to X^2\Sigma^+$ and $2^4\Pi \to 1^4\Sigma^+$ transitions are also computed by the SC method, as shown in Fig. 4. The QM and SC cross-sections exhibit a good agreement over the entire energy interval, and the SC cross-sections almost reproduce the baseline of those determined by the QM method. However, the SC method could not produce the cross-sections at high collision energies due to the Franck–Condon principle (Franck & Dymond 1926; Condon

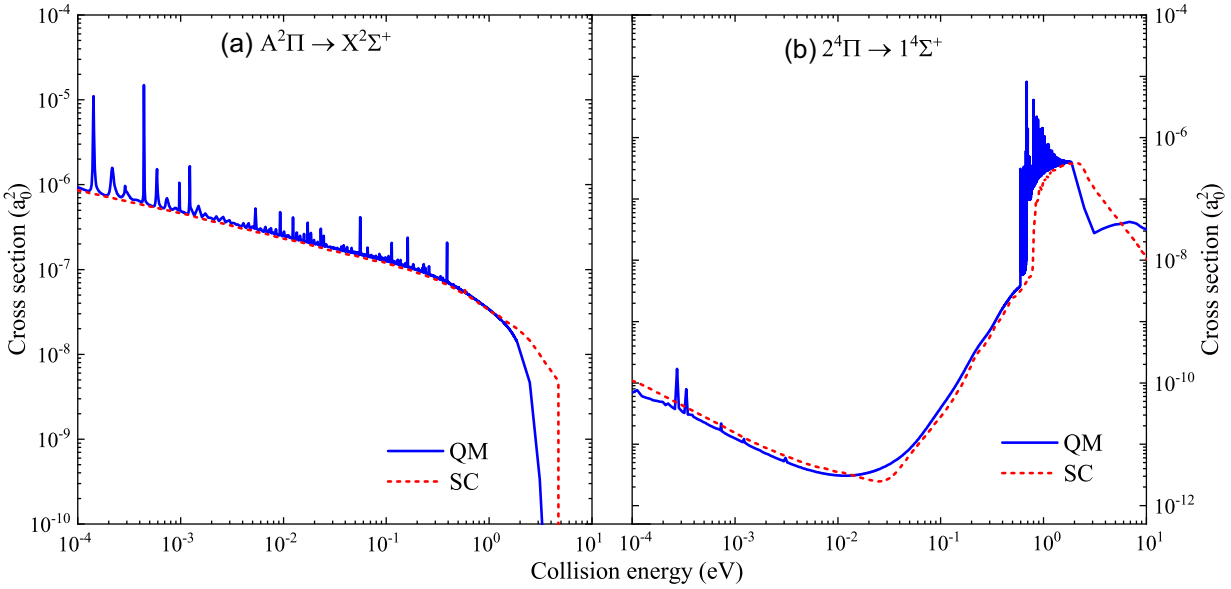

Figure 4. Cross-sections for the (a) $A^2\Pi \rightarrow X^2\Sigma^+$ and (b) $2^4\Pi \rightarrow 1^4\Sigma^+$ transitions.

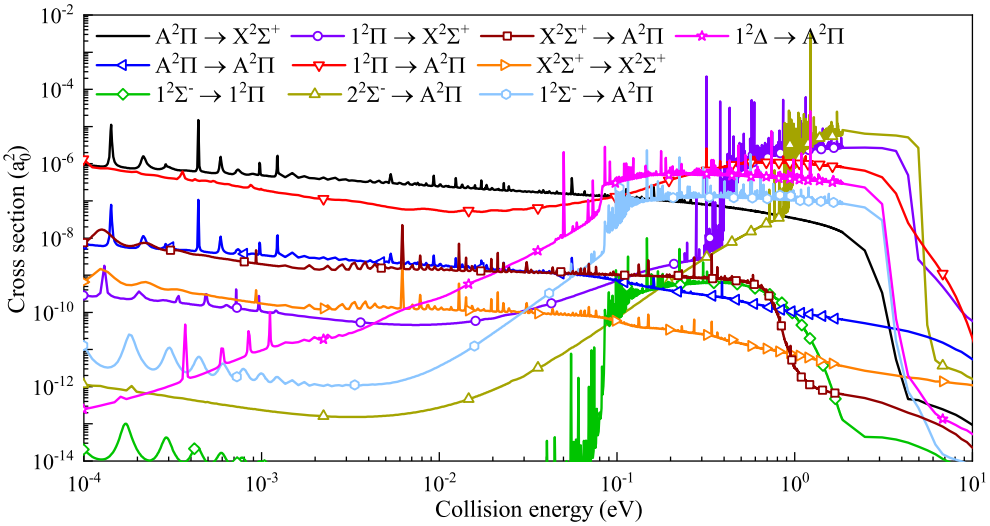

Figure 5. Cross-sections for the studied transition systems between doublet states by the QM method.

1928). Besides, the resonance contribution is crucial at high collision energies but not considered in the SC method.

The radiative association cross-sections for each transition of AlO in Table 2 are calculated using the QM method, as shown in Figs 5 and 6. Note that the cross-sections exhibit many peaks that come from the resonances. In addition, we also explored the $1^2\Pi \rightarrow 1^2\Delta$, $1^2\Pi \rightarrow 1^2\Sigma^-$, $2^2\Sigma^- \rightarrow 1^2\Sigma^-$, $2^4\Sigma^- \rightarrow 1^4\Sigma^-$, and $2^4\Pi \rightarrow 1^4\Pi$ transitions but found their cross-sections were insignificant.

At low collision energies (<0.1 eV), the cross-sections for the $A^2\Pi \rightarrow X^2\Sigma^+$ transition are large. As the energies increase, the cross-sections for 12 transitions, such as the $1^2\Pi \rightarrow X^2\Sigma^+$, $2^2\Sigma^- \rightarrow A^2\Pi$, $1^2\Delta \rightarrow A^2\Pi$, $2^4\Pi \rightarrow 1^4\Delta$, $2^4\Pi \rightarrow 1^4\Sigma^+$, and $1^4\Pi \rightarrow 1^2\Delta$ transitions, exhibit sharp jumps due to the barriers on the PECs of the $1^2\Sigma^-$, $1^2\Pi$, $1^2\Delta$, $2^2\Sigma^-$, $1^4\Pi$, and $2^4\Pi$ states in Fig. 1. For example, the cross-sections for the $1^2\Delta \rightarrow A^2\Pi$ and $2^4\Pi \rightarrow 1^4\Sigma^+$ transitions go up rapidly at the collision energies of about 0.084 and 0.732 eV, respectively. This behaviour can be generally found in other similar electronic transition systems, such as the $D^1\Delta \rightarrow A^1\Pi$ and $e^3\Sigma^- \rightarrow a^3\Pi$ transitions of MgO (Bai, Qin & Liu 2021) and the $1^4\Sigma_g^+ \rightarrow a^4\Sigma_u^+$ system of N_2^+ (Qin, Bai & Liu 2021). Finally, the results show that the cross-sections for the $1^2\Pi \rightarrow X^2\Sigma^+$ and $2^2\Sigma^- \rightarrow A^2\Pi$ transitions are dominant for high energies. For the other six transitions, the cross-sections decrease monotonically as the energies increase.

3.3 Rate coefficients

The rate coefficients for the radiative association of AlO through 19 transitions are computed by averaging the cross-sections over a Maxwellian velocity distribution for temperatures in the range of 10–10 000 K, as shown in Fig. 7. The rate coefficients for the transitions between doublet states are larger within the calculated temperature range. As expected from the cross-sections, the dominant transitions are the $A^2\Pi \rightarrow X^2\Sigma^+$, $1^2\Delta \rightarrow A^2\Pi$, $1^2\Pi \rightarrow X^2\Sigma^+$, and $2^2\Sigma^- \rightarrow A^2\Pi$ transitions. The rate coefficients for these four transitions and the total rate coefficients for all transitions are shown in Fig. 8,

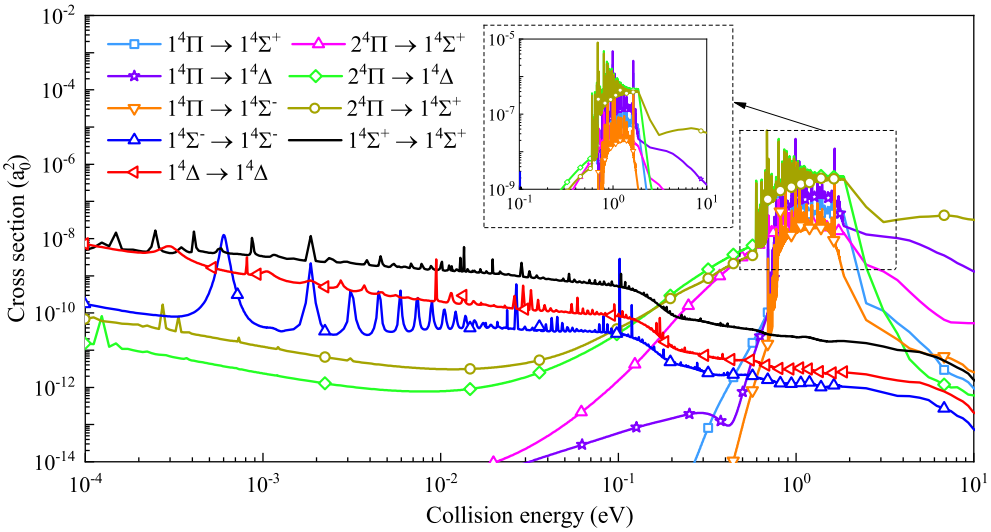

Figure 6. Cross-sections for the studied transition systems between quartet states by the QM method.

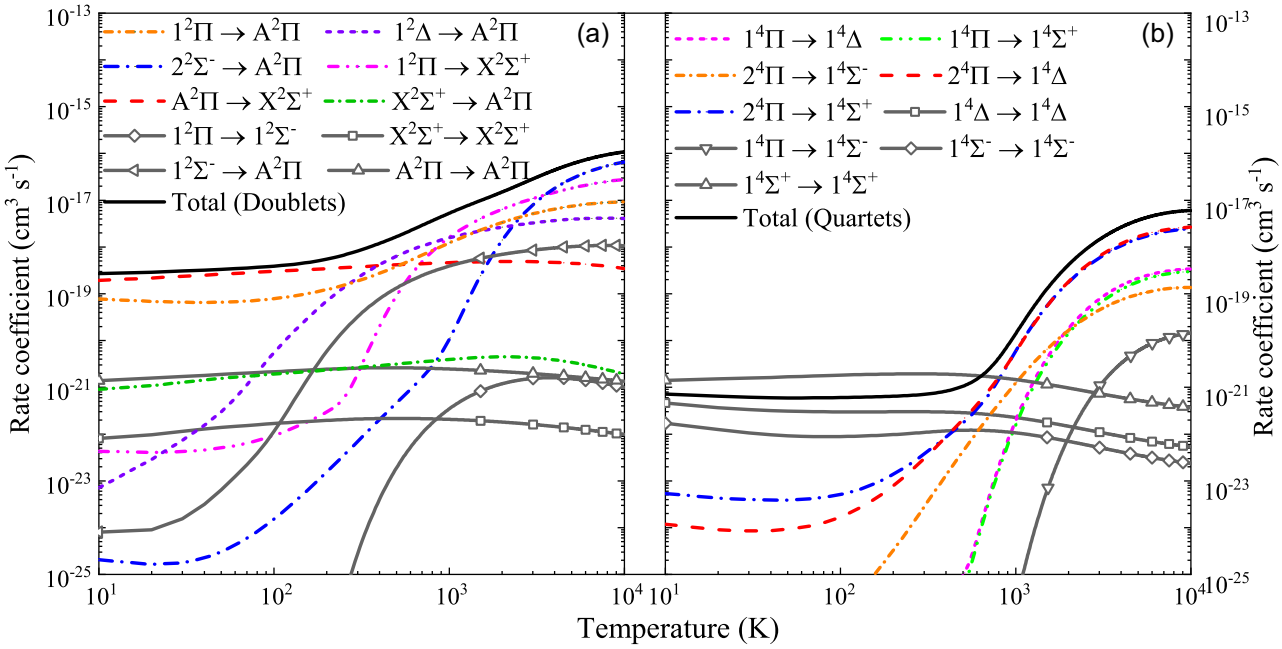

Figure 7. Rate coefficients for the radiative association of AlO through the transitions between (a) doublet and (b) quartet states.

where the $A^2\Pi \rightarrow X^2\Sigma^+$ transition is dominant at low temperatures (<390 K), the $1^2\Delta \rightarrow A^2\Pi$ and $1^2\Pi \rightarrow X^2\Sigma^+$ transitions dominate for the temperatures of 390–990 and 990–3530 K, respectively, and the $2^2\Sigma^- \rightarrow A^2\Pi$ transition is dominant at high temperatures (>3530 K).

Compared with the total rate coefficients from Ceccatto (2012), there is a discrepancy between our and Ceccatto's results. Our results are larger at high temperatures due to the resonance contribution considered in our calculation. These resonance contributions are significant for the cross-sections at high collision energies, as shown in Figs 5 and 6. Another reason is that the rate coefficients calculated by Ceccatto (2012) considered only three transitions, including the $A^2\Pi \rightarrow X^2\Sigma^+$, $1^2\Pi \rightarrow A^2\Pi$, and $1^2\Pi \rightarrow X^2\Sigma^+$ transitions. Meanwhile, the extrapolation of experimental data were employed in the calculation of Ceccatto (2012), which may lead inaccurate PECs on the high-energy levels because of only low-energy levels measured in experiments.

The total rate coefficients for the radiative association of AlO through all transitions in Table 2 can be approximated using the three-parameter Kooij function (within 1 per cent), which is expressed as

$$k(T) = A\left(\frac{T}{300}\right)^{\alpha} e^{-\beta/T}. \quad (6)$$

where A, α, and β are fitting parameters.The rate coefficient curves are divided into three temperature ranges, and the fitting parameters are summarized in Table 3. The fitted rate coefficient deviates less than 1 per cent from our calculated ones.

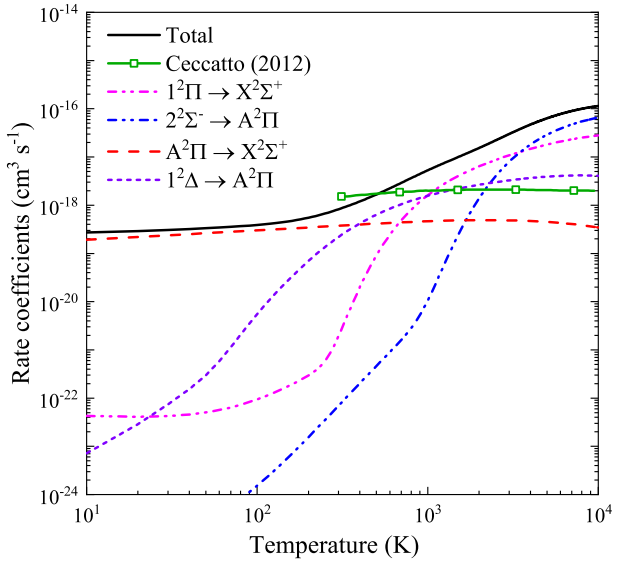

Figure 8. Rate coefficients for the radiative association of AlO. Note that 'Total' denotes the total rate coefficients obtained by all transitions in Table 2, and Ceccatto (2012) denotes the rate coefficients obtained by the $A^2\Pi \rightarrow X^2\Sigma^+$, $1^2\Pi \rightarrow A^2\Pi$, and $1^2\Pi \rightarrow X^2\Sigma^+$ transitions in the calculation of Ceccatto (2012).

Table 3. Fit parameters according to Kooij function (equation (6)) for the total rate coefficients.

T(K)	A (cm^3 s^{-1})	α	$\beta(K)$
10–4000	6.9034×10^{-19}	1.6281	−51.3148
4000–7000	1.8649×10^{-16}	0.0370	5906.3382
7000–10 000	1.0225×10^{-15}	− 0.3769	8701.4476

4 CONCLUSIONS

In this work, we calculated the cross-sections and rate coefficients for the formation of AlO by radiative association of oxygen and aluminium atoms in their electronic ground states. As the basis for calculating cross-sections, the PECs for 12 electronic states and the TDMs and PDMs for 19 transitions were obtained by the icMRCI + Q/aug-cc-pCV5Z-DK methodology. A large set of the PECs, TDMs, and PDMs can extend the available molecular data on AlO. The cross-sections for these transitions were then obtained by the QM method. Finally, the rate coefficients were computed for the temperatures in the range of 10–10 000 K.

The radiative association cross-sections for the $A^2\Pi \rightarrow X^2\Sigma^+$ transitions are large at low collision energies (<0.1 eV). As the collision energies increase, the cross-sections for the $1^2\Delta \rightarrow A^2\Pi$, $1^2\Pi \leftarrow X^2\Sigma^+$, and $2^2\Sigma^- \rightarrow A^2\Pi$ transitions are dominant due to the barrier on the PECs. Similarly, the rate coefficients are dominated by the $A^2\Pi \rightarrow X^2\Sigma^+$, $1^2\Delta \rightarrow A^2\Pi$, $1^2\Pi \rightarrow X^2\Sigma^+$, and $2^2\Sigma^- \rightarrow A^2\Pi$ transitions, where the $A^2\Pi \rightarrow X^2\Sigma^+$ transition is dominant at low temperatures (<390 K), the $1^2\Delta \rightarrow A^2\Pi$ and $1^2\Pi \rightarrow X^2\Sigma^+$ transitions dominate for the temperatures of 390–840 and 990–3530 K, respectively, and the $2^2\Sigma^- \rightarrow A^2\Pi$ transition is dominant at high temperatures (>3530 K).

The total rate coefficients for the radiative association of AlO are of the order of 2.73×10^{-19}–1.14×10^{-16} cm^3 s^{-1} for the temperatures of 10–10 000 K. The calculated values can be used to investigate the chemical evolution of the aluminium oxide dust formation in the photospheres of the oxygen-rich AGB star.

DECLARTION OF INTERESTS

The authors declare that they have no known competing financial interests or personal relationships that could have influenced the work reported in this paper.

ACKNOWLEDGEMENTS

The support provided by the National Natural Science Foundation of China (52106098, 51421063) is greatly acknowledged. ZQ also acknowledges the support provided by the Natural Science Foundation of Shandong Province (ZR2021QE021), Postdoctoral Innovation Project of Shandong Province, and Postdoctoral Applied Research Project of Qingdao City. The scientific calculations in this paper have been done on the HPC Cloud Platform of Shandong University.

DATA AVAILABILITY STATEMENT

All data are available in this paper. The cross sections and rate coefficients can be obtained online at https://dr-zhi-qin.github.io/personal/Database.html. The supplementary material includes the PECs of 12 electronic states in Fig. 1, the TDMs for the transitions in Fig. 2, the PDMs for the electronic states in Fig. 3, the rate coefficients for the transition processes in Table 2, and the total rate coefficients.

REFERENCES

Andreazza C., de Almeida A., 2014, MNRAS, 437, 2932
Andreazza C., de Almeida A., Vichietti R., 2018, MNRAS, 477, 548
Bai T., Qin Z., Liu L., 2021, MNRAS, 500, 2496
Banerjee D., Misselt K., Su K., Ashok N., Smith P., 2007, ApJ, 666, L25
Ceccatto D. T., 2012, Master thesis, Paulista State University
Chang T. Y., 1967, Rev. Mod. Phys., 39, 911
Cherchneff I., Lilly S., 2008, ApJ, 683, L123
Condon E. U., 1928, Phys. Rev., 32, 858
Das A. K., Thakkar A. J., 1999, J Phys.: At. Mol. Opt. Phys., 31, 2215
De Beck E., Decin L., Ramstedt S., Olofsson H., Menten K., Patel N., Vlemmings W., 2017, A&A, 598, A53
de Jong W. A., Harrison R. J., Dixon D. A., 2001, J. Chem. Phys., 114, 48
Franck J., Dymond E., 1926, Trans. Faraday Soc., 21, 536
Fuentealba P., 2004, Chem. Phys. Lett., 397, 459
Gobrecht D., Cherchneff I., Sarangi A., Plane J., Bromley S., 2016, A&A, 585, A6
Golubev N. V., Bezrukov D. S., Gustafsson M., Nyman G., Antipov S. V., 2013, J. Phys. Chem. A, 117, 8184
Hansson A., Watson J. K. G., 2005, J. Mol. Spectrosc., 233, 169
Honjou N., 2010, J. Mol. Struct.: Theochem, 939, 59
Huber K. P., Herzberg G., 1979, Molecular Spectra and Molecular Structure. Van Nostrand Reinhold Company, New York
Johnson B. R., 1977, J. Chem. Phys., 67, 4086
Johnson B. R., 1978, J. Chem. Phys., 69, 4678
Keenan P., Deutsch A., Garrison R., 1969, ApJ, 158, 261
Knowles P. J., Werner H. J., 1985, Chem. Phys. Lett., 115, 259
Knowles P. J., Werner H. J., 1988, Chem. Phys. Lett., 145, 514
Kovba V. M., Topol I. A., 1986, J. Mol. Struct: Theochem, 137, 65
Kramida A., Ralchenko Y., Reader J., NIST ASD Team, 2021, Available at: https://physics.nist.gov/asd, 2021-7-1
Launila O., Jonsson J., 1994, J. Mol. Spectrosc., 168, 1
Lengsfield B. H., Liu B., 1982, J. Chem. Phys., 77, 6083
Liu H., Shi D., Sun J., Zhu Z., 2013, Spectrochim. Acta A, 101, 400
London F., 1937, Trans. Faraday Soc., 33, 8
Merrill P. W., Deutsch A. J., Keenan P. C., 1962, ApJ, 136, 21
Nyman G., Gustafsson M., Antipov S. V., 2015, Int. Rev. Phys. Chem., 34, 385
Onaka T., De Jong T., Willems F., 1989, A&A, 218, 169

Partridge H., Langhoff S. R., Lengsfield B. H.,, III, Liu B., 1983, J. Quant. Spectrosc. Radiat. Transfer, 30, 449
Qin Z., Bai T., Liu L., 2021, MNRAS, 507, 2930
Saksena M. D., Deo M. N., Sunanda K., Behere S. H., Londhe C. T., 2008, J. Mol. Spectrosc., 247, 47
Sarangi A., Cherchneff I., 2013, ApJ, 776, 107
Schamps J., 1973, Chem. Phys., 2, 352
Speck A., Barlow M., Sylvester R., Hofmeister A., 2000, A&AS, 146, 437
Takigawa A., Kamizuka T., Tachibana S., Yamamura I., 2017, Sci. Adv., 3, eaao2149
Tenenbaum E., Ziurys L. M., 2009, ApJ, 694, L59
Towle J. P., James A. M., Bourne O. L., Simard B., 1994, J. Mol. Spectrosc., 163, 300
Van Heijnsbergen D., Demyk K., Duncan M., Meijer G., Von Helden G., 2003, Phys. Chem. Chem. Phys., 5, 2515
Watson J. K. G., 2008, J. Mol. Spectrosc., 252, 5
Werner H. J., Knowles P. J., 1988, J. Chem. Phys., 89, 5803
Werner H.-J. et al., 2015, Molpro, Version 2015.1: A Package of Ab Initio Programs. TTI GmbH Stuttgart, Stuttgart
Woon D. E., Dunning T. H.,, Jr, 1995, J. Chem. Phys., 103, 4572
Yoshimine M., McLean A. D., Liu B., 1973, J. Chem. Phys., 58, 4412
Zenouda C., Blottiau P., Chambaud G., Rosmus P., 1999, J. Mol. Struct.: Theochem, 458, 61

SUPPORTING INFORMATION

Supplementary data are available at *MNRAS* online.

Supplemental materials.zip

Please note: Oxford University Press is not responsible for the content or functionality of any supporting materials supplied by the authors. Any queries (other than missing material) should be directed to the corresponding author for the paper.

This paper has been typeset from a TEX/LATEX file prepared by the author.